J. Fluid Mech. (2009), *vol.* 620, *pp.* 313–332.
doi:10.1017/S0022112008004606 Printed in the United Kingdom

Drift and deformation of oil slicks due to surface waves

K. H. CHRISTENSEN[1]† AND E. TERRILE[2]

[1]Department of Geosciences, University of Oslo, N-0315 Oslo, Norway
[2]Department of Applied Mathematics and Theoretical Physics, University of Cambridge, Cambridge CB3 0WA, UK

(Received 17 December 2007 and in revised form 13 October 2008)

We present a theoretical model for the wave-induced drift and horizontal deformation of an oil slick. The waves and the mean flow are coupled through the influence of the mean flow on the concentration of slick material, which in turn determines the damping rate of the waves and hence the transfer of momentum from the waves to the mean flow. We also briefly discuss a simplified version of the model that can be used when remote sensing data are available. With this simpler model the wave-induced forcing of the mean flow is obtained directly from observations of the wave field, hence knowledge of any specific slick properties is not required.

1. Introduction

Surface capillary-gravity waves are effectively damped by an oil slick due to the greatly increased shear in the surface boundary layer caused by the slick (Lamb 1932; Dorrestein 1951). When the waves are damped, a part of the forward momentum in the waves is transferred to a mean flow/drift current. The wave damping effect is most pronounced for capillary-gravity waves that have typical wavelengths of 1–10 cm. Since the backscatter from the sea surface is mainly due to these short waves, a slick is represented as a dark patch in radar images, which makes radars a useful tool for detecting oil spills. The presence of an oil slick can also be noted as a profound dip in the high-frequency part of the wave spectrum (Alpers & Hühnerfuss 1988).

For a large slick there are no short waves in the interior, the wave damping effect being too strong, so that only the long waves (of more than a few meters length, say) can pass relatively unhindered. Thus, the main transfer of momentum from the waves to the mean flow takes place in a narrow band that runs along the edge of the slick, and the forcing of the mean flow will be much stronger in this band than that in the interior (see figure 1). Furthermore, many types of slicks possess a strong resistance against a change in total area, but a limited resistance against a change in shape (e.g. Hansen & Ahmad 1971). Since the induction of drift currents will vary greatly over the slick, we may expect that the horizontal shape of the slick will change on the same time scale as that of the slick drift velocity. We will refer to this change in shape as a deformation of the slick. In previous studies, the wave-induced changes in surfactant concentration have been neglected as far as the wave dynamics are concerned (e.g. Christensen 2005 and references therein). It is the purpose of this paper to examine

† Email address for correspondence: k.h.christensen@geo.uio.no

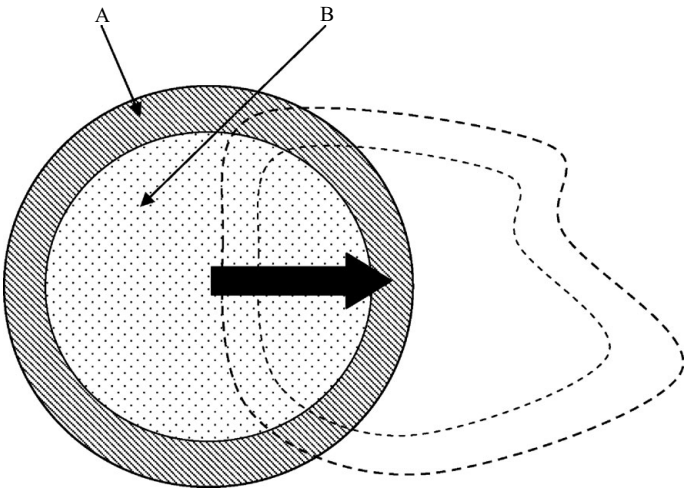

FIGURE 1. Short capillary-gravity waves are effectively damped in the region A. The wave-induced stresses in this region will vary in both size and direction, with the effect that the horizontal shape of the slick will change with time. Although the longer waves can pass relatively unhindered (propagating from left to right), they will induce stresses in the propagation direction that will be approximately constant in both regions A and B. Assuming that the time scales of the drift and the deformation are similar, the time development is likely to be as indicated (at least qualitatively).

the two-way coupling between the waves and the oil slick and to present a more complete model for the drift and deformation of the slick due to surface waves.

In this study, we therefore focus on the small-scale dynamics in the surface boundary layer, and we apply a fairly simple description of the wave field. That is, we do not take into account the stochastic dispersion of slick material in a random wave field (e.g. Herterich & Hasselmann 1982; Balk 2006; Vucelja *et al.* 2007), but in our simulations we assume that all components of the wave field are completely known. Neither do we consider steep waves prone to breaking, nor other effects of wave-induced turbulence, such as Langmuir turbulence (e.g. McWilliams *et al.* 1997; Polton & Belcher 2007).

In this paper, we model the oil slick as an insoluble elastic monolayer. The procedure, however, is general and the validity of the model can be extended by formulating alternative conservation laws for the slick material. We build our theory on results for the Lagrangian mean motion based on the method of Weber (1983). For the mean drift current we make the usual eddy viscosity assumption, allowing the eddy viscosity to vary with depth and the waves to be (implicitly) represented by a directional wave spectrum (Jenkins 1989). What we obtain is a new model for the drift of oil slicks in which the effect of the drift velocities on the slick properties are accounted for. The results are correct to second order in wave amplitude and represent the lowest order drift problem. That is, all mean velocities scale as the Stokes drift, which is proportional to the wave steepness squared times the phase velocity of the waves. In particular, our analysis is valid for small wave steepness $a\kappa \ll 1$, where a is the wave amplitude and κ the wavenumber, and when the ratio between the oscillatory surface boundary layer width d and the wavelength is small, expressed by $\kappa d \ll 1$. For the short capillary-gravity waves considered here, the latter ratio is of $O(10^{-2})$ (e.g. Dorrestein 1951). Since the analysis is based on a direct Lagrangian approach the results are strictly speaking only valid for a short time.

Numerical simulations for a short time period show that the waves rapidly cause a significant redistribution of slick material.

The outline of this paper is as follows: In § 2, we present the model, formulating the equations governing the slick properties, the waves and the mean flow in §§ 2.1, 2.2 and 2.3, respectively. In § 3, we show numerical solutions for the mean concentration of slick material, the wave-induced stresses on the slick and the drift and deformation of a slick for a few simple cases. Further, in § 4.1 we discuss the combined use of remote sensing data and a simplified version of the model. Finally, § 4.2 contains concluding remarks and some suggestions for future studies.

2. Mathematical formulation

The fluid motion is three-dimensional, and we take the x- and y-axes to be aligned with the undisturbed sea surface. The z-axis is vertical and positive upwards, and the unit vectors in the (x, y, z)-directions are $(\boldsymbol{i}, \boldsymbol{j}, \boldsymbol{k})$, respectively. We assume that the fluid is incompressible and homogeneous with constant density ρ. The system is rotating about the z-axis with an angular velocity $f/2$, where f is the Coriolis parameter. Here, we denote periodic quantities with zero mean by a tilde $\tilde{(\ )}$, while mean values are denoted by an overbar $\overline{(\ )}$. The depth is taken to be infinite. There are two different time scales in this problem. One is proportional to the wave period, and the other is the time scale of the much slower wave-induced drift velocities. The effect of the Earth's rotation can be neglected as far as the waves are concerned (Pollard 1970), but the Coriolis force can be important on the longer time scale of the drift, or if the slick is very large (Christensen & Weber 2005*b*).

Let the undisturbed surface level be given by $z=0$. We consider plane and progressive surface waves, and write the wave field as a sum of Fourier components $\tilde{\zeta}_\kappa$:

$$\tilde{\zeta}_\kappa = a_\kappa(x, y, t)\cos(kx + ly - \omega_\kappa t + \delta_\kappa) + O\left(a_\kappa^2\kappa\right). \tag{2.1}$$

Here, $\kappa = \sqrt{k^2 + l^2}$ is the wavenumber, ω_κ is the wave frequency and δ_κ is a random constant phase shift uniformly distributed between $[0, 2\pi]$. The unit vector in the direction of wave propagation is $\boldsymbol{i}_\kappa = \kappa^{-1}(k\boldsymbol{i} + l\boldsymbol{j})$. The sea surface is given by

$$z = \zeta = \overline{\zeta} + \sum_\kappa \tilde{\zeta}_\kappa, \tag{2.2}$$

defining the mean surface elevation $\overline{\zeta}(x, y, t)$, and the sum is taken over all the Fourier components. This sum will in practice be substituted with the equivalent integral representation for a continuous directional wave spectrum, but the above notation will be used throughout for clarity. We assume that the wave amplitude and propagation direction 'upstream' of the slick is known for each wave component. It is clear that the slick will have a sheltering effect so that a wave that passes through the area covered by the slick will re-enter the region outside the slick with reduced amplitude. Since we consider plane waves, we will only need to match the wave field in the interior of the slick with the external field at the edge where the waves enter. As far as the waves are concerned no specific matching condition is needed at the edges where the waves leave the slick. Note that the present analysis includes the case of a non-contaminated surface. In the numerical simulations presented in § 3 we solve the governing equations in the entire domain, so that also the drift velocities outside this region are accounted for.

The Eulerian and Lagrangian velocities at any particular point in time and space must be equal. If the Lagrangian velocity of a particle starting from the position $\boldsymbol{x}_L$ at time $t = t_0$ is $\boldsymbol{u}_L(\boldsymbol{x}_L, t_0)$, say, then the Eulerian velocity $\boldsymbol{u}_E$ of the same particle at a later time can be found from the relation

$$\boldsymbol{u}_L(\boldsymbol{x}_L, t) = \boldsymbol{u}_E\left(\boldsymbol{x}_L + \int_{t_0}^{t} \boldsymbol{u}_L(\boldsymbol{x}_L, t')\,\mathrm{d}t', t\right). \tag{2.3}$$

By using a Taylor series expansion (e.g. Phillips 1977, § 3.3)

$$\boldsymbol{u}_L(\boldsymbol{x}_L, t) = \boldsymbol{u}_E(\boldsymbol{x}_L, t) + \left(\int_{t_0}^{t} \boldsymbol{u}_E(\boldsymbol{x}_L, t')\,\mathrm{d}t'\right) \cdot \nabla_L \boldsymbol{u}_E(\boldsymbol{x}_L, t) + O(a^3), \tag{2.4}$$

where $\nabla_L = \partial/\partial \boldsymbol{x}_L$. Substituting the Lagrangian coordinates $\boldsymbol{x}_L$ with Eulerian coordinates $\boldsymbol{x}$ introduces an additional correction term of $O(a^3)$, which we will neglect here. Certain limitations for the validity of the analysis then apply, however, which is further discussed in § 2.3.

For a fluid particle, the mean forward momentum associated with the wave (2.1) is represented by the Stokes drift, which is the mean value of the second term on the right-hand side of (2.4). For deep water waves the Stokes drift is given by

$$\overline{\boldsymbol{v}}_S = u_0 \exp(2\kappa z)\boldsymbol{i}_\kappa, \tag{2.5}$$

with $u_0 = a_\kappa^2 \omega_\kappa \kappa$. The total mean Lagrangian velocity $\overline{\boldsymbol{v}}_L$ is the sum of the Stokes drift and a Eulerian component $\overline{\boldsymbol{v}}_E$ such that

$$\overline{\boldsymbol{v}}_L = \overline{\boldsymbol{v}}_E + \sum_{\kappa} \overline{\boldsymbol{v}}_S. \tag{2.6}$$

The oil slick is advected by the horizontal Lagrangian velocity at the surface, which we will denote by $\overline{\boldsymbol{v}}_L^{(0)}$.

2.1. *Properties of the oil slick*

The oil slick is represented by the concentration of slick material $\Gamma(x, y, t)$. Here we consider insoluble and elastic monolayers, although we discuss possible generalizations in § 4. The dynamically significant slick variables are the surface tension σ and the elastic modulus E. The elastic modulus is defined as

$$E \equiv -\frac{\mathrm{d}\sigma}{\mathrm{d}(\ln \Gamma)}. \tag{2.7}$$

The relation between Γ and σ depends on the slick material and must be determined from experiments (e.g. Mass & Milgram 1998). For our purposes it is sufficient to assume that

$$\sigma = G(\Gamma), \tag{2.8}$$

and that G is a known function.

Because the slick is insoluble and stays on the surface at all times, the problem of finding Γ can be reduced to a two-dimensional problem involving only the horizontal surface velocities, that is, we project all quantities related to the problem onto the xy-plane. We denote the horizontal component of the Eulerian velocity at the surface as $\boldsymbol{v}_E^{(\zeta)}$. Applying the Reynolds transport theorem we then obtain the following relation between the fluid velocities and the concentration Γ (for the equivalent Lagrangian formulation see Weber & Saetra 1995):

$$\frac{\partial \Gamma}{\partial t} = -\nabla \cdot \left(\Gamma \boldsymbol{v}_E^{(\zeta)}\right). \tag{2.9}$$

For periodic wave motion $\tilde{\boldsymbol{v}}_\kappa$ corresponding to (2.1) (see for example Hansen & Ahmad 1971), we obtain by expanding $\tilde{\boldsymbol{v}}_\kappa(z=\tilde{\zeta}_\kappa)$ in powers of $\tilde{\zeta}_\kappa$:

$$\overline{\tilde{\boldsymbol{v}}_\kappa(z=\tilde{\zeta}_\kappa)} = \overline{\tilde{\boldsymbol{v}}_\kappa(z=0) + \frac{\partial \tilde{\boldsymbol{v}}_\kappa}{\partial z}(z=0)\tilde{\zeta}_\kappa + O\left(a_\kappa^2\omega\kappa\right)} = \overline{\boldsymbol{v}}_S(z=0)/2 + O\left(a_\kappa^2\omega\kappa\right). \quad (2.10)$$

We now assume that Γ can be split into periodic components and a slowly varying component that incorporates the equilibrium value:

$$\Gamma = \overline{\Gamma} + \sum_\kappa \tilde{\Gamma}_\kappa. \quad (2.11)$$

From Weber & Saetra (1995) we obtain correct to $O(a^2)$ for the fluctuating components:

$$\tilde{\Gamma}_\kappa = (\kappa\overline{\Gamma}/\omega_\kappa)\tilde{\boldsymbol{v}}_\kappa(z=0) + O(a^2). \quad (2.12)$$

From (2.6), (2.9), (2.10) and (2.12) we obtain correct to $O(a^2)$ that

$$\frac{\mathrm{D}^{(0)}\overline{\Gamma}}{\mathrm{d}t} = -\overline{\Gamma}\,\boldsymbol{\nabla}\cdot\,\overline{\boldsymbol{v}}_L^{(0)}, \quad (2.13)$$

where we have defined a material derivative for mean variables evaluated at the surface:

$$\frac{\mathrm{D}^{(0)}}{\mathrm{d}t} = \frac{\partial}{\partial t} + \overline{\boldsymbol{v}}_L^{(0)}\cdot\boldsymbol{\nabla}\,. \quad (2.14)$$

Equation (2.13) for the mean concentration of slick material has previously been neglected in theoretical studies of the wave-induced drift. The result is simple, although not surprising given the similarities between the approach used here and the generalized Lagrangian-mean theory of Andrews & McIntyre (1978). In fact, the result (2.13) could have been obtained directly by considering (2.9) for $\overline{\Gamma}$ using the wave solutions $\tilde{\boldsymbol{v}}_\kappa$ evaluated at $(\boldsymbol{x} + \int \tilde{\boldsymbol{v}}_\kappa\,\mathrm{d}t, \zeta_\kappa)$.

The mean displacement $\overline{\boldsymbol{X}}$ of the oil slick is governed by

$$\frac{\mathrm{D}^{(0)}\overline{\boldsymbol{X}}}{\mathrm{d}t} = \overline{\boldsymbol{v}}_L^{(0)}. \quad (2.15)$$

It is not strictly necessary to solve for $\overline{\boldsymbol{X}}$, since the properties of the oil slick are completely determined by $\overline{\Gamma}$. It is nevertheless useful to know the mean displacement. If the material derivative in (2.13) is simply treated as a time derivative, the value of $\overline{\Gamma}$ can be found by integrating the right-hand side forwards in time. Since the value obtained is a Lagrangian quantity, it should be assigned to the position $(x, y) = \overline{\boldsymbol{X}}$ given by integrating (2.15) forwards in time in a similar way.

2.2. *Properties of the waves*

The wavelength of each component is $\lambda_\kappa = 2\pi/\kappa$. If the horizontal extent of the slick is L, we require that $L > \lambda_\kappa$, for all wave components. For wavelengths approximately equal to the slick length or longer it has been shown experimentally that the slick is passively advected by the inviscid Stokes drift and the steady streaming corresponding to a non-contaminated (slick free) surface (e.g. the discussions in Weber 2001; Wong & Law 2003). For wavelengths that are about half the length of the slick or less, the present analysis is valid (Law 1999; Christensen & Weber 2005*a*).

At the surface there is a thin oscillatory boundary layer of width γ_κ^{-1}, where $\gamma_\kappa = \sqrt{\omega_\kappa/2\nu_0}$ and ν_0 is the kinematic (eddy) viscosity. This eddy viscosity will in general be different from the eddy viscosity used in the drift equations. The reason

for this is that the wave motion has a much shorter time scale than the corresponding drift velocity. The mean currents will therefore respond to larger turbulent eddies with longer time scales than the turbulent eddies affecting the waves (see the discussion in Jenkins & Ardhuin 2004). There is a net production of second-order vorticity in the surface boundary layer, with a corresponding downward diffusion of mean momentum (Longuet-Higgins 1953). It is by this mechanism that momentum is transferred from the waves to the mean current, at a rate which strongly depends on the dynamical conditions at the surface.

Due to the excitation of longitudinal elastic (dilational) waves in the slick, the capillary-gravity waves are very effectively damped (Dorrestein 1951; Lucassen 1968). All the essential details concerning the slick/wave dynamics can be described using a non-dimensional elasticity parameter $\mathscr{E}_\kappa$, defined by

$$\mathscr{E}_\kappa = \frac{E\kappa^2\gamma_\kappa}{\rho\omega_\kappa^2}. \tag{2.16}$$

For $\mathscr{E}_\kappa = 1$ the wave damping has a maximum due to resonance between the forced elastic wave and the capillary-gravity wave (Christensen 2005).

We will assume that the time dependence in a_κ is due to the slow redistribution of slick material and that the wave field outside the slick is steady in time. The rate of change with time of the wave amplitude at any particular point must then be due to the local change in slick material concentration. Hence the temporal growth/decay rate β should scale as

$$\beta \propto \frac{1}{\overline{\Gamma}}\frac{\partial\overline{\Gamma}}{\partial t}. \tag{2.17}$$

We may assume that the mean drift velocities change on the same horizontal scale as the waves and that the mean drift velocity scales as the Stokes drift u_0 (e.g. Christensen 2005). If the spatial attenuation rate of the waves is α, we then obtain from (2.13) that

$$\beta/\alpha \propto u_0. \tag{2.18}$$

For cases where both the spatial and temporal growth/decay rates of the waves are important we have in general (Gaster 1962)

$$\beta/\alpha = c_g, \tag{2.19}$$

where c_g is the group velocity of the waves. Since $u_0 \ll c_g$, we will neglect temporal growth/decay of the wave amplitudes in the linear part of the analysis and assume our problem is one of spatial attenuation. For the derivation of the drift equations we will treat a_κ as steady in time, while in practice both the amplitude and the spatial damping rate will be slowly varying functions of (x, y, t).

We assume that for each wave component the amplitude changes along the propagation direction according to

$$\frac{\partial a_\kappa}{\partial\xi} = -\alpha_\kappa a_\kappa, \tag{2.20}$$

where we have defined the directional derivative $\partial/\partial\xi = \boldsymbol{i}_\kappa \cdot \nabla$.

The effect of slick elasticity is most pronounced with regard to the damping rate. Defining $F = 1 - 2\mathscr{E}_\kappa + 2\mathscr{E}_\kappa^2$, the damping rate is locally determined by the elasticity

parameter such that (Lucassen-Reynders & Lucassen 1969)

$$\alpha_\kappa = \frac{c_p^{(\kappa)}\kappa^2}{2c_g^{(\kappa)}\gamma_\kappa}\left[\frac{\mathscr{E}_\kappa^2}{F} + \frac{\kappa}{\gamma_\kappa}\frac{2(1-\mathscr{E}_\kappa)}{F}\right]. \tag{2.21}$$

Here $c_p^{(\kappa)} = \omega_\kappa/\kappa$ is the phase velocity and $c_g^{(\kappa)} = \partial\omega_\kappa/\partial\kappa$ is the group velocity of the wave component in question. The elasticity parameter is in turn locally determined by the concentration of slick material Γ. In practice the value of $\mathscr{E}$ will be obtained from (2.7), (2.8) and (2.16) using the mean values $\overline{\sigma}$ and $\overline{\Gamma}$.

The ratio between the wavenumber and the inverse oscillatory boundary layer thickness is κ/γ_κ and is typically of the order 10^{-1} to 10^{-2} for capillary-gravity waves. Wave dispersion is given by

$$\omega_\kappa^2 = \left[g\kappa + (\overline{\sigma}/\rho)\kappa^3\right](1 + O(\kappa/\gamma_\kappa)), \tag{2.22}$$

where g is the acceleration due to gravity, and the negligible $O(\kappa/\gamma_\kappa)$-term is due to the presence of the slick (e.g. Christensen 2005). The fact that the slick elasticity does not have any significant effect on wave dispersion shows that gravity and surface tension are still the dominating restoring forces in the vertical direction, even for a contaminated surface.

2.3. *Properties of the wave drift*

As shown in the previous section, the wave amplitude variation over the slick can be determined once we know the concentration of slick material $\overline{\Gamma}$. Now we need to find the Lagrangian surface drift $\overline{\boldsymbol{v}}_L^{(0)}$ to close the problem and solve for $\overline{\Gamma}$. As in the previous section, we will not go into details concerning the derivation of the governing equations, instead we apply known solutions for the Lagrangian mean motion. A brief overview is also given in the Appendix.

While the linearized equations of motion are formally identical in the Lagrangian and Eulerian descriptions, it is not so for the mean drift. It is necessary to apply some sort of surface-following coordinates in order to find the correct forcing terms for the mean drift velocities because the width of the surface boundary layer is usually small compared to the wave amplitude (Longuet-Higgins 1953).

The Lagrangian drift velocity can in general be split into three different parts (e.g. Craik 1982):

$$\overline{\boldsymbol{v}}_L = \overline{\boldsymbol{u}} + \sum_\kappa(\overline{\boldsymbol{v}}_S + \overline{\boldsymbol{v}}_v). \tag{2.23}$$

Here $\overline{\boldsymbol{v}}_v$ is the steady streaming in the oscillatory boundary layer, which can be found from a detailed analysis in Lagrangian or curvilinear coordinates, and $\overline{\boldsymbol{u}}$ is a transient Eulerian drift current. Due to the waves there is a net production of vorticity in the oscillatory boundary layer that causes a mean stress on the slick. In the absence of external forces, this stress must be balanced by the viscous shear due to the Eulerian mean current $\overline{\boldsymbol{u}}$, and momentum spreads downwards by turbulent or viscous diffusion. If a direct Lagrangian approach is used, we find that the horizontal drift velocities to $O(a^2)$ are governed by an equation of the form (see Appendix)

$$\mathscr{L}\{\overline{\boldsymbol{v}}_L\} = \sum_\kappa \mathscr{L}\{(\overline{\boldsymbol{v}}_S + \overline{\boldsymbol{v}}_v)\} + \boldsymbol{P}^{(h)} - f\boldsymbol{k}\times\overline{\boldsymbol{v}}_L, \tag{2.24}$$

where $\mathscr{L}\{\,\}$ is a linear operator in t and the Lagrangian space coordinates, and $\boldsymbol{P}^{(h)}$ is a second-order pressure gradient force due to changes in the mean surface level. The Stokes drift and the steady streaming are thus particular solutions of the drift

equation. Both the first two terms $\overline{\boldsymbol{v}}_S$ and $\overline{\boldsymbol{v}}_v$ on the right-hand side of (2.24) are obtained from the linear solutions. By use of (2.23) we obtain from (2.24)

$$\mathscr{L}\{\overline{\boldsymbol{u}}\} = \boldsymbol{P}^{(h)} - f\boldsymbol{k} \times \overline{\boldsymbol{v}}_L. \tag{2.25}$$

At this point we make use of a property of the transformation between the Eulerian and Lagrangian descriptions, namely that

$$x = x_L + O(a), \qquad y = y_L + O(a), \qquad z = z_L + O(a), \tag{2.26}$$

where (x_L, y_L, z_L) are the Lagrangian space coordinates (Pierson 1962; Weber 1983). Thus, we will take the $O(a^2)$ Lagrangian equations of motion and continuity and simply replace the Lagrangian coordinates with their Eulerian counterparts. The error we make will be of $O(a^3)$, and we obtain an expression for the Lagrangian momentum balance, recast into Eulerian coordinates, which is correct to $O(a^2)$. By using this substitution, the validity of our model will be limited to a time period proportional to $(a_\kappa \kappa \omega_\kappa)^{-1}$. We obtain, however, an expression for the Lagrangian momentum balance, which is more correct from a Newtonian point of view. It should also be pointed out that the relevant forcing terms can also be obtained by use of curvilinear coordinate systems (e.g. Law 1999) or a GLM-approach (e.g. Broström, Christensen & Weber 2008), for which the short time limitation does not apply.

For the spatially damped surface waves we considered here, we have

$$\mathscr{L} = \frac{\partial}{\partial t} + \frac{\partial}{\partial z_L}\left(\overline{\nu}\frac{\partial}{\partial z_L}\right) \approx \frac{\partial}{\partial t} + \frac{\partial}{\partial z}\left(\overline{\nu}\frac{\partial}{\partial z}\right). \tag{2.27}$$

Here we have introduced a turbulent eddy viscosity $\overline{\nu}$ that may differ from the effective viscosity that causes wave damping (see the discussion in § 2.2, and also Jenkins & Ardhuin 2004).

If we neglect the contribution from the steady streaming in the Coriolis force, the equation governing $\overline{\boldsymbol{u}}$ becomes

$$\frac{\partial \overline{\boldsymbol{u}}}{\partial t} - \frac{\partial}{\partial z}\left(\overline{\nu}\frac{\partial \overline{\boldsymbol{u}}}{\partial z}\right) + f\boldsymbol{k} \times \overline{\boldsymbol{u}} = -g\nabla\overline{\zeta} - f\boldsymbol{k} \times \sum_\kappa \overline{\boldsymbol{v}}_S. \tag{2.28}$$

This equation is essentially equivalent to that of Jenkins (1989), the exception being that we allow for a horizontal pressure gradient force. Also, Jenkins models the momentum transfer from the waves to the mean flow with a source term in the momentum equation. Here we follow Longuet-Higgins (1969) and force the mean flow through a virtual wave stress applied at the surface.

It should be noted that we have neglected any nonlinear term that may originate from products between different wave components. It has been shown that roll motion is induced in the case of intersecting waves of equal length and phase (e.g. Melsom 1992), which for instance could have some effect on some of the numerical examples shown later on. Intersecting waves produce a pattern of standing waves that gives rise to a spanwise periodicity in the forcing terms. Craik (1982) has shown that a unidirectional flow is unstable to such disturbances in the forcing. The roll motion is a consequence of the periodic forcing and continuity, and hence the time needed to develop this motion is much longer than the wave period. The neglect of this effect implies that we do not allow the waves to locally cancel or amplify each other in accordance with the pattern of standing waves they produce. Apart from the practical difficulties involved in properly calculating all the forcing terms (for instance, we need to know the phase-constant δ_κ of each component), the two main reasons for not

including this effect here are: (i) The waves induce relatively rapid changes in the slick properties, and the properties of the wave field change accordingly. Hence the forcing of the mean flow at any particular point is not steady in time, but can be assumed changing on a time scale similar to or less than that needed to establish the roll motion. (ii) The wave-induced currents are vertically sheared, hence even if roll motion starts to develop through a deeper layer in some region, the slick will eventually drift away and further development will be inhibited. Nevertheless, spanwise periodic motion has been observed in the laboratory in situations when the slick has been prevented from drifting (e.g. Mockros & Krone 1968; Gushchin & Ermakov 2003), and the possibility that the flow can be unstable should therefore be kept in mind, in particular with regard to large and slowly drifting slicks.

For deep-water waves the equation of continuity to $O(a^2)$ is†

$$\nabla \cdot \overline{\boldsymbol{v}}_L = \sum_\kappa \frac{\partial}{\partial t}\left(a_\kappa^2 \kappa^2 \mathrm{e}^{2\kappa z}\right). \tag{2.29}$$

It follows that the Lagrangian mean drift current in general is divergent, and consequently the mean surface elevation is not always equal in the Eulerian and Lagrangian descriptions (Longuet-Higgins 1986). Neglecting the contribution from the boundary layer streaming, we define the Eulerian transport $\boldsymbol{M}_E$ and the Stokes transport $\boldsymbol{M}_S$ as

$$\boldsymbol{M}_E = \rho \int_{-\infty}^{0} \overline{\boldsymbol{u}}\, \mathrm{d}z, \tag{2.30a}$$

$$\boldsymbol{M}_S = \rho \int_{-\infty}^{0} \overline{\boldsymbol{v}}_S\, \mathrm{d}z. \tag{2.30b}$$

Since the vertical velocity at the surface to $O(a^2)$ is given by $\partial\overline{\zeta}/\partial t$, we obtain from (2.29) by vertical integration:

$$\rho \frac{\partial}{\partial t}\left(\overline{\zeta} - \sum_\kappa s_\kappa\right) = -\nabla \cdot (\boldsymbol{M}_E + \sum_\kappa \boldsymbol{M}_S), \tag{2.31}$$

where we have defined $s_\kappa = (a_\kappa^2 \kappa)/2$. The quantity s_κ is the difference between the Eulerian and Lagrangian mean surface elevation (e.g. McIntyre 1988; Jenkins & Ardhuin 2004). We note that a time-dependent wave field will in general contribute to (2.31) both through $\boldsymbol{M}_S$ and s_κ, while the latter contribution vanish if the waves (and hence the slick properties) do not change with time.

To solve for $\overline{\boldsymbol{u}}$ we need two boundary conditions. First, we must require that the velocities tend to zero at great depths:

$$\overline{\boldsymbol{u}} \to 0, \qquad z \to -\infty. \tag{2.32}$$

The dynamic boundary condition at the surface is (Weber & Saetra 1995; Christensen 2005)

$$\rho\overline{\nu}\frac{\partial \overline{\boldsymbol{u}}}{\partial z} = \sum_\kappa \boldsymbol{\tau}_\kappa - \nabla\overline{\sigma}, \qquad z = 0. \tag{2.33}$$

† This result follows from the equation of continuity in the Lagrangian description of motion, see for example Weber (2003), his equation (2.5), which is our (A 8). The same result can also be obtained using GLM theory, see for example McIntyre (1988), his equation (1) with $\xi_{i,i} = 0$.

There is a constant redistribution of momentum from the waves to the mean flow due to the dissipation of wave energy in the boundary layer. Here we have introduced the virtual wave stress $\boldsymbol{\tau}_\kappa$ to represent this redistribution (Longuet-Higgins 1969, also see the Appendix for details). The virtual wave stress can be connected to the momentum loss in the waves. We will make use of the mean wave momentum equation of Weber (2001), which relates the virtual wave stress to the mean wave momentum flux

$$\boldsymbol{\tau}_\kappa = -c_g^{(\kappa)} \frac{\partial \boldsymbol{M}_S}{\partial \xi} = \rho \left(\frac{\alpha_\kappa}{\kappa} \right) c_g^{(\kappa)} u_0 \boldsymbol{i}_\kappa. \tag{2.34}$$

Here we have made use of (2.5), (2.20) and (2.30). With (2.34) we now have a complete set of equations for the transient Eulerian mean drift $\overline{\boldsymbol{u}}$. To obtain an expression for $\overline{\boldsymbol{v}}_L^{(0)}$ correct to $O(a^2)$ we will also need the surface value of the steady streaming. For the oil slicks we considered here, we have (Weber & Saetra 1995; Christensen 2005)

$$\overline{\boldsymbol{v}}_v(z=0) = u_0 \left[\frac{\mathscr{E}_\kappa(4 - 5\mathscr{E}_\kappa)}{2F} - \frac{\kappa}{\gamma_\kappa} \right] \boldsymbol{i}_\kappa. \tag{2.35}$$

The Lagrangian velocity at the surface is obtained by adding (2.35) and the Stokes drift velocity to $\overline{\boldsymbol{u}}$ such that

$$\overline{\boldsymbol{v}}_L^{(0)} = \overline{\boldsymbol{u}}(z=0) + \sum_\kappa \left[\overline{\boldsymbol{v}}_S(z=0) + \overline{\boldsymbol{v}}_v(z=0) \right]. \tag{2.36}$$

With (2.36) we close the problem for the drift and deformation of the oil slick.

3. Results

We present here a few numerical simulations to illustrate the two-way coupling between the slick and the waves. For simplicity, we have neglected Coriolis forces and changes in the mean surface elevation, setting $\overline{\zeta} = 0$. By (2.31) this simplification implies that we neglect gradients in the volume fluxes. Since we only simulate the drift and deformation during a short time interval ($t < 20$ s), the induced flows are quite shallow and the spatial differences in the total volume transport are small. It should nevertheless be noted that possible edge effects, in which mean surface level changes can be important, are neglected (for example with regard to the so-called Reynolds Ridge, e.g. Harper & Dixon 1974).

3.1. *Configuration of the numerical model*

A domain of 3×3 m has been considered. The oil slick is initially circular with a radius of 1 m and centred in the domain. A Crank–Nicolson scheme is used to solve (2.28). Equation (2.13) is solved using a first-order Rusanov scheme (Rusanov 1961). The grid sizes have been chosen small enough to avoid effects of the discretization on the solution. The horizontal grid size is 2 cm, while the vertical grid size is approximately 0.5 cm. The time step used is 0.1 s, and the results were converged for the total duration of the simulations.

In the simulations we have used a combination of three different wave components. The wave field is characterized by a dominant wave propagating in the x-direction with a wavelength $\lambda = 15$ cm and an initial wave steepness $a\kappa = 0.1$ and two shorter waves with $\lambda = 5$ cm and with initial wave steepness $a\kappa = 0.03$. These two shorter waves are propagating at an angle of $\pm 45^\circ$ to the x-axis (see the right panel in figure 2). In the simulations we have imposed the wave field instantaneously on the entire domain. For this reason we have also assumed that both the Stokes drift and the

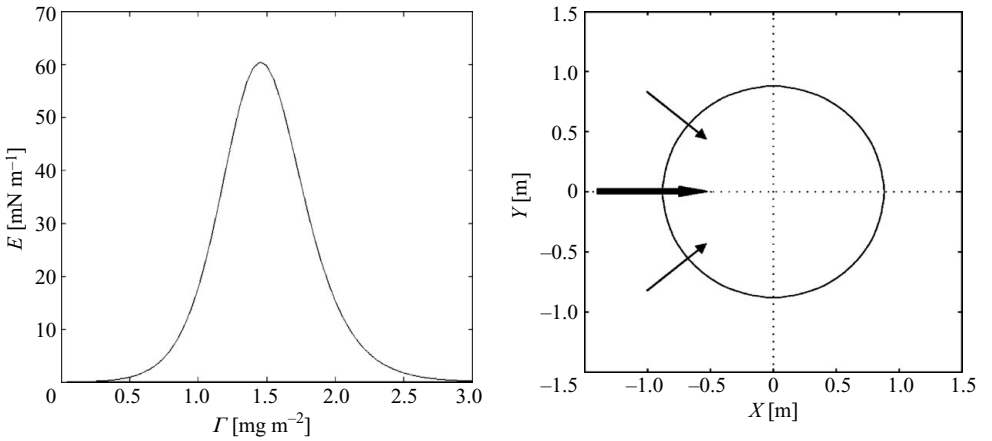

FIGURE 2. Left panel shows $E(\overline{\Gamma})$ from (3.1). Note that the slick elasticity has a maximum, and tends to zero for higher concentrations (due to collapse of the monolayer). The right panel shows the computational domain and the initial shape of the slick. The arrows illustrate the propagation direction of the waves used in the simulations.

boundary layer streaming are present from the outset, using $\overline{\boldsymbol{u}}(t=0)=0$ as the initial condition and $\overline{\boldsymbol{u}}(z=-\lambda_{max}/2)=0$ is used as bottom boundary condition. The flow is assumed to be laminar, and the kinematic viscosity is that of water $\nu=10^{-6}\,\mathrm{m^2\,s^{-1}}$.

Function (2.8) that relates the surface tension and the surfactant concentration has been constructed to fit the experimental results of Vogel & Hirsa (2002) for oleyl alcohol, a chemical which is commonly used in laboratory experiments. From (2.7) we have then computed the following relation between the elastic modulus E and the mean concentration $\overline{\Gamma}$:

$$E(\overline{\Gamma}) = \tfrac{1}{2}\overline{\Gamma}\sigma_r\Delta\sigma_s\left\{1-\tanh^2\left[\Delta\sigma_s(\overline{\Gamma}-\Gamma_m)\right]\right\}, \tag{3.1}$$

where $\sigma_r=33.9\,\mathrm{m^2\ mg^{-1}}$, $\Gamma_m=1.4\,\mathrm{mg\,m^{-2}}$ and $\Delta\sigma_s=2.5\ \mathrm{mN\,m^{-1}}$. Function (3.1) is depicted in figure 2.

3.2. *Model results*

To obtain the results shown in figures 3–5, we have only considered the dominating wave that propagates in the x-direction. Figure 3 shows the concentration of slick material and the slick elasticity for a transect along $y=0$ m. The left panel shows the initial values, which are symmetric with respect to the y-axis. The right panel shows the values after 18 s, and it is clearly seen that this symmetry is lost. At the 'upstream' end of the slick, the gradients are smoother, which is due to the divergence in the horizontal mean velocities: The velocities are higher under the slick. At the other end of the slick there is a concentration maximum, and a corresponding maximum in the elasticity. It should be noted that the initial concentration is rather weak, and the value of the elasticity parameter $\mathscr{E}_\kappa$ is of the order 10^{-1}.

The changes in the slick material concentration have consequences for the waves. Figure 4 shows the damping coefficient from (2.21) both initially and after 18 s. Left panel shows a transect along $y=0$ m, while the right panel shows a transect along $y=0.7$ m. If the feedback from the mean flow on the mean concentration had been neglected, the initial values would have been passively advected with the mean flow, and the mean wave-induced stress exerted on any particular point on the slick would

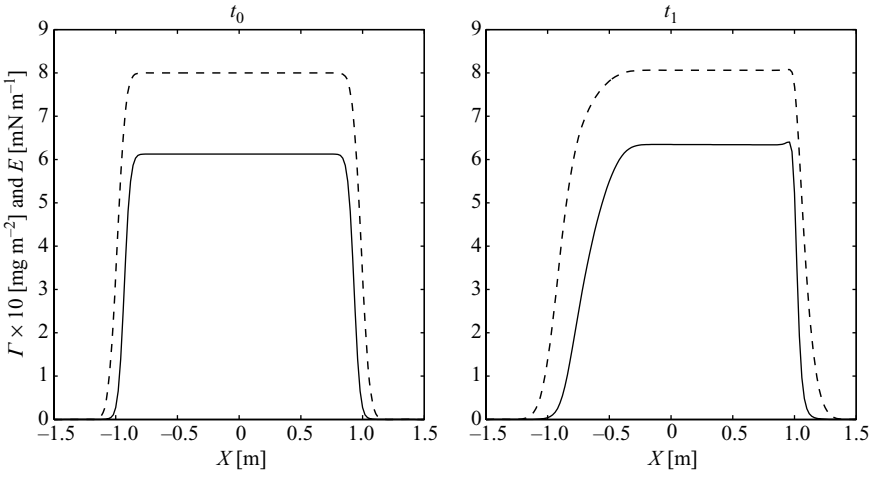

FIGURE 3. Spatial variation of the concentration $\overline{\Gamma}$ (dashed line) and the corresponding elasticity E (solid line) along the x coordinate at $y = 0$, using only the dominant wave component. The left panel shows initial values, while the right panel for $t = 18$ s.

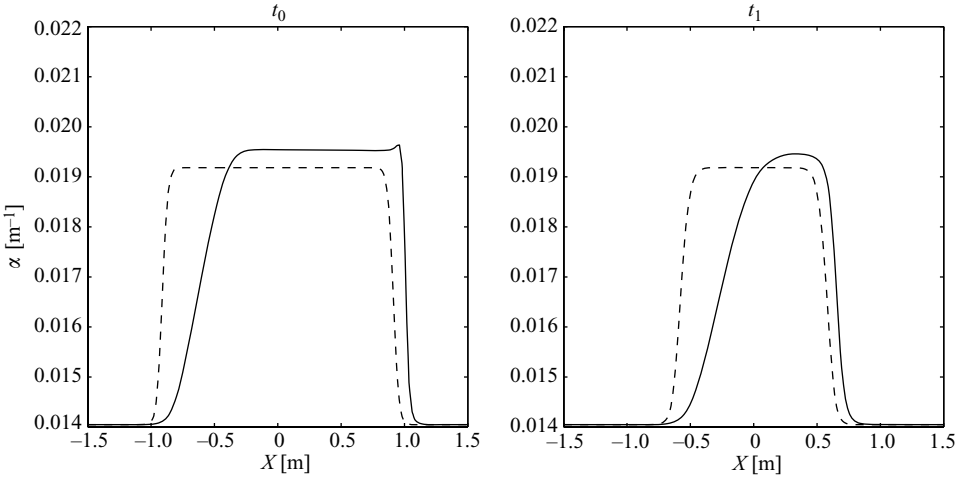

FIGURE 4. Spatial variation of the wave damping coefficient α_κ corresponding to figure 3. Dashed lines show initial values, and the solid lines the values for $t = 18$ s. The left panel shows the variation along $y = 0$ m, while the right panel shows the variation along $y = 0.7$ m.

have been constant. As seen here, however, the concentration changes in such a way that maximum wave damping is found towards the 'downstream' end of the slick. Furthermore, the maximum value of the damping coefficient increases because the mean concentration increases, and, hence, also the value of the elasticity parameter $\mathscr{E}_\kappa$. For higher initial concentration the wave-induced changes in mean concentration may lead to lower values of the damping coefficient since this coefficient has a maximum for $\mathscr{E}_\kappa = 1$.

The surface stress in (2.33) that accelerates the mean flow contains two terms: the virtual wave stress and the gradient of the mean surface tension. In figure 5 these two terms are compared for a transect along $y = 0$ m. It is evident that the mean surface tension gradient is negligible, hence the dynamic boundary condition (2.33) is well

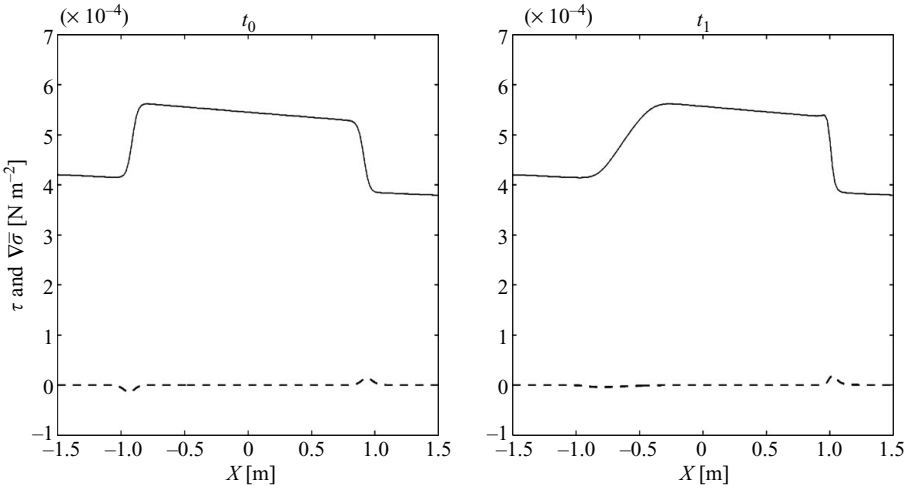

FIGURE 5. Comparison between the x-component of the virtual wave stress τ (solid line) and the surface tension gradient $\nabla\overline{\sigma}$ (dashed line) corresponding to figure 3. Initial values are shown in the left panel, while the right panel shows the results for $t = 18$ s.

approximated by

$$\rho\overline{\nu}\frac{\partial\overline{\boldsymbol{u}}}{\partial z} = \sum_{\kappa}\boldsymbol{\tau}_{\kappa}, \qquad z = 0. \tag{3.2}$$

In figure 6 the x-component of the virtual wave stress is shown for two different types of slicks. The left column shows results for an elastic slick, while the right column shows results for an inextensible (inelastic) slick. If the slick is truly inextensible, we obtain from (2.13) that the total area of the slick is conserved since the Lagrangian surface velocities are non-divergent. In the inextensible limit $E \to \infty$, the wave damping rate becomes

$$\alpha_{\kappa} = \frac{c_p^{(\kappa)}\kappa^2}{4c_g^{(\kappa)}\gamma_{\kappa}}, \tag{3.3}$$

which means that the damping rate is a function of the wave parameters only. This value of the damping rate is sometimes used to calculate wave attenuation rates and wave-induced stresses in real slicks (e.g. Phillips 1977, § 3.4). In the simulations shown here, although the mean concentration may be changing, we only keep track of the slick position using (2.15). Thus we actually simulate an inelastic slick that can be deformed, which is of course not the case for the plastic sheets often used in laboratory experiments (e.g. Law 1999). The use of (3.3) only implies, however, that the wave motion is suppressed in such a way that a no-slip condition applies for this motion, which can for example be the case in the marginal ice zone (e.g. Christensen & Weber 2005*b*). In the upper panels only the dominant wave has been used, while in the middle panels we consider all three components. In the lower panels we show results for the two shorter waves. Judging from the differences between the upper and middle panels we can conclude that the inelastic slick is quite insensitive to the shorter waves. It is also clear from the lower panels that the effect of the shorter waves is stronger near the slick edges, which is simply because these short waves more quickly dissipate under the slick. The upper and middle panels indicate that the elastic slick is compressed, while the inelastic slick attains a characteristic bell shape.

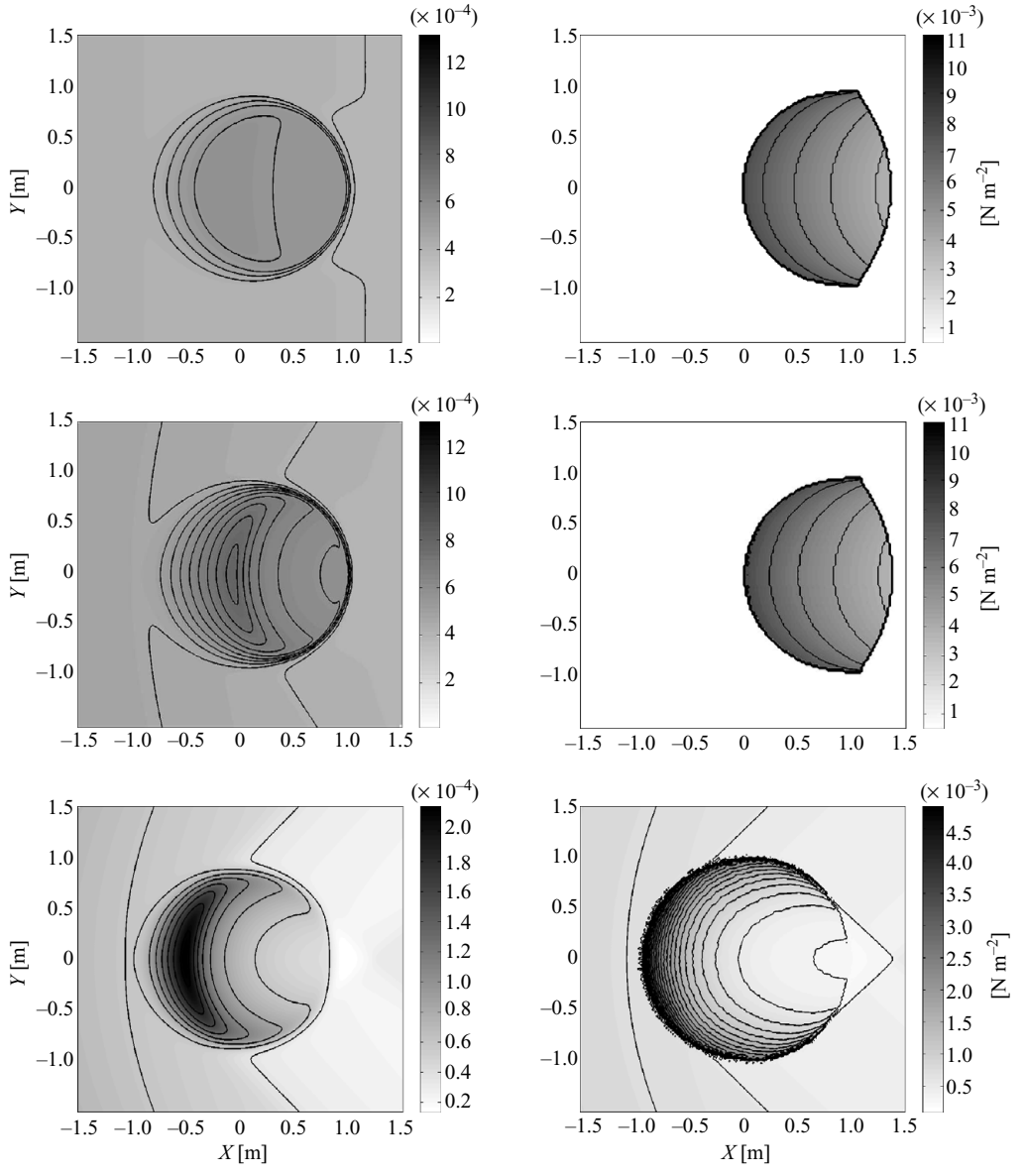

FIGURE 6. The distributions of the x-component of the virtual wave stress are shown for two different types of slicks and for three different combinations of the waves. The left panel shows results for an elastic slick that initially had a constant concentration of slick material equal to the initial value shown in figure 3. The right panel shows results for an inelastic slick. In the upper panel we have only considered the dominating long wave component, while the middle panel shows the results from using all three wave components. The lower panel shows the results from using the two short wave components (note the different scales). All results are for $t = 18$ s.

In practice, the slick may collapse in regions of strong convergence, and part of the slick material can be mixed with the fluid below.

In figure 7, we show an example of slick deformation by plotting isolines for the slick material concentration. The left panel shows the deformation of the elastic slick from figure 6 under the influence of all three waves. As in figure 3 we can see that

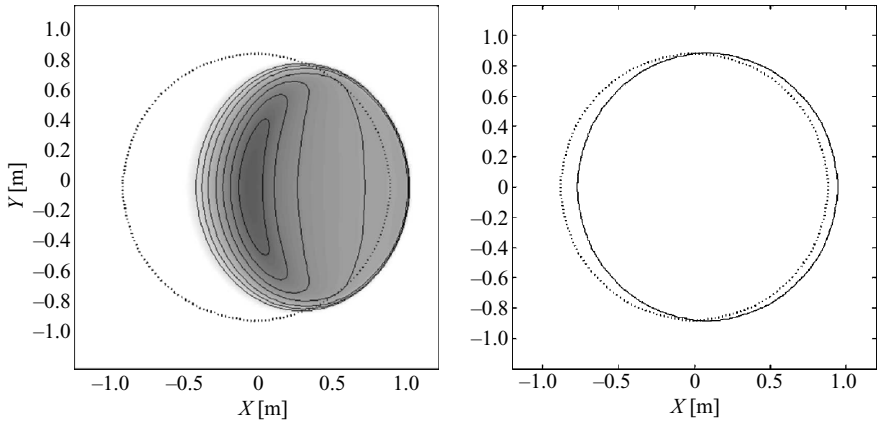

FIGURE 7. The drift and deformation of an elastic slick is shown in the left panel, and for a clean surface in the right panel. All three wave components have been used in the simulations. Isolines (steps of $0.01\,\mathrm{mg\,m^{-2}}$) for the slick material concentration $\overline{\Gamma}$ are shown in the left panel for $t = 18$ s. The maximum value of $\overline{\Gamma}$ is approximately $0.84\,\mathrm{mg\,m^{-2}}$. The dotted lines show the initial shape of the slick/material surface. In the right panel, the solid line marks the boundary of the material surface for $t = 18$ s.

the gradients are smoother at the edge where the waves enter the slick, but we find a concentration maximum near the upstream edge that was not present when only the dominant wave was considered in figure 3 (also compare with the left panels of figure 6). The right panel shows the corresponding deformation of a material surface element in the case of a clean water surface. The shape of this surface element is also changed somewhat because of the viscous attenuation of the waves and the corresponding mean drift velocities. However, the shorter waves have a stronger influence on the elastic slick compared to the clean water surface and the former is more compressed in the y-direction.

Our results are qualitatively in agreement with observations by Marmorino *et al.* (2008), who used satellite imagery to examine slick motion characteristics. Although they primarily considered natural sea slicks, the wave-slick dynamics are the same (e.g. Mass & Milgram 1998). Marmorino *et al.* (2008) also found convergence zones near the downstream edge and a divergence zone near the upstream edge of the slick. More detailed comparisons between our results and their observations cannot be made since we have not taken into account wind effects in this study. Our results indicate, however, that observations of sea slick 'banding' and rapid redistribution of slick material need not be only due to Langmuir circulation cells, but that the wave-slick dynamics in the surface boundary layer may play an equally important role.

4. Discussion

4.1. *Oil spill surveillance and remote sensing*

Remote sensing is often used to discover and monitor oil spills at sea. The wave dampening effect of the oil causes a marked reduction in backscatter from the sea surface, hence an oil spill can be recognized as a dark patch on radar images. A major problem, however, is that it is difficult to distinguish between slicks made from different materials. For instance, on a radar image a natural sea slick may look very much the same as oil released from a ship. Without a means to determine what

chemicals the slick is composed of, we cannot model the relation between the slick material concentration and surface tension (2.8). We need to know this relation in order to calculate the wave damping rates (2.21), which are subsequently used to calculate the mean wave-induced stresses.

If the properties of the slick are unknown but observational data for the sea surface elevation are available, a simplified version of the model can be constructed as follows: From data of $\zeta(x, y, t)$ we can extract the wave spectrum and the wave amplitudes $a_\kappa(x, y, t)$. The wave damping rates $\alpha_\kappa(x, y, t)$ can then be directly computed from these data even though we do not know any properties of the slick. From these quantities we can calculate the virtual wave stress in (2.34) and force the mean flow through the boundary condition (2.33). If we neglect the gradient of the surface tension in this boundary condition and the steady streaming in (2.36), we have effectively removed all slick parameters from the system of equations. We still retain the influence of the slick implicitly through (2.34).

This approach is equivalent to that of Weber (2001) for breaking waves and Weber, Broström & Saetra (2006) for the integrated wave-induced transports in the surface layer of the ocean. This simpler model could prove useful for making short-term forecasts (nowcasts) of oil spill trajectories in limited areas of special interest. In practice we would need data of high resolution in both time and space. This is not a serious limitation, however, since radar systems that should be able to provide the necessary coverage are already in commercial use (for example WaMoS and MIROS/Wavex).

4.2. *Concluding remarks*

The presented theory describes the two-way coupling between an oil slick and surface waves. Provided that the rheological properties of the slick are known, a complete set of equations governing the drift and deformation of an oil slick is given. In traditional oil spill trajectory models the drift velocity of the oil slick is often taken to be proportional to the wind speed/current speed (e.g. ASCE 1996), implying that the stresses acting on the slick are horizontally uniform on smaller scales. As we show here, this cannot be the case when waves are present since the wave-induced stresses vary greatly over the slick. Furthermore, we show that the changes in the slick material concentration caused by the mean flow lead to significant changes in the wave properties, which has previously been neglected in theoretical models. The presented theory is of course approximate and several important aspects of real flows need to be further investigated. In particular we mention soluble slick material, background currents and the influence of the wind.

For the case of soluble slick material, conservation laws for other types of slick material may be formulated that can replace (2.9). We obtain a closed set of equations as long as the concentration of slick material only depends on the waves and the mean drift velocities, since we explicitly solve for these quantities.

It is also of interest to calculate the effects of background currents on the wave-induced drift. Background currents will affect the wave frequencies and amplitudes, and horizontally sheared currents will deform the slick. As background currents we may also count the orbital velocities in long waves with wavelengths at least as large as the slick.

Finally, the effects of the wind are important. The action of the wind may prevent wave damping altogether even in the presence of an oil slick: both (2.21) for the attenuation rate of the waves and (2.34) for the virtual wave stress will contain

terms representing atmospheric forcing (Saetra 1998; Weber *et al.* 2006). While these results should be relatively straightforward to incorporate in the present model, there are other, more complex, mechanisms that must also be investigated. A direct consequence of the suppression of the short waves is that the sea surface roughness is locally reduced. Hence, the wind profile in the atmospheric boundary layer will become horizontally non-uniform with possible consequences for the drift of the slick. For example, Welander (1963) suggested that the reduction in sea surface roughness creates a convergent wind field over the slick. The atmospheric boundary layer over waves is a field of active research, and incorporating the effects of the wind will be the next step in constructing a robust theory for the drift and deformation of an oil slick.

The authors wish to thank Ms Giovanna Grosso for help with the numerical solution methods, and Professor Jan Erik Weber for helpful discussions. KHC gratefully acknowledges financial support from the Research Council of Norway through Grant No. 171215.

Appendix. Lagrangian analysis

The presented theory is based on the results of a detailed analysis in which a Lagrangian description of the motion is used. The details can be found in Christensen (2005), but a short summary is given here for completeness.

In a direct Lagrangian approach we assign a reference position (x_L, y_L, z_L) to each fluid particle, and use these as independent space coordinates. The position (X, Y, Z) at time t of a fluid particle then becomes a function of the Lagrangian space coordinates, such that $X = X(x_L, y_L, z_L, t)$ and so on. The position of any particular fluid particle is then written as

$$X = x_L + x(x_L, y_L, z_L, t), \tag{A 1}$$

$$Y = y_L + y(x_L, y_L, z_L, t), \tag{A 2}$$

$$Z = z_L + z(x_L, y_L, z_L, t). \tag{A 3}$$

Similarly, for the pressure P we write

$$P = -\rho g z_L + p(x_L, y_L, z_L, t). \tag{A 4}$$

Spatial derivatives in the Eulerian coordinates are transformed according to

$$\frac{\partial \phi}{\partial x} = J(\phi, Y, Z), \quad \frac{\partial \phi}{\partial y} = J(X, \phi, Z), \quad \frac{\partial \phi}{\partial z} = J(X, Y, \phi), \tag{A 5}$$

where J is the Jacobian of the transformation. We neglect Coriolis forces and consider a single wave component that propagates in the x-direction; hence we assume that all quantities are independent of the y-coordinate. The Navier–Stokes equations and the continuity equation correct to second order in the wave steepness, are (e.g. Weber 2003):

$$\begin{aligned} &\frac{\partial^2 x}{\partial t^2} - \nu \nabla_L \frac{\partial x}{\partial t} = -\frac{1}{\rho} \frac{\partial}{\partial x_L}(p + \rho g z) - \frac{1}{\rho} J(p, z) \\ &+ \nu \left[J\left(\frac{\partial^2 x}{\partial t \partial x_L}, z \right) + J\left(x, \frac{\partial^2 x}{\partial t \partial z_L} \right) + \frac{\partial}{\partial x_L} J\left(\frac{\partial x}{\partial t}, z \right) + \frac{\partial}{\partial z_L} J\left(x, \frac{\partial x}{\partial t} \right) \right], \end{aligned} \tag{A 6}$$

$$\frac{\partial^2 z}{\partial t^2} - \nu\nabla_L \frac{\partial z}{\partial t} = -\frac{1}{\rho}\frac{\partial}{\partial z_L}(p + \rho g z) - \frac{1}{\rho}J(x, p) - gJ(x, z) + \nu\left[J\left(\frac{\partial^2 z}{\partial t \partial x_L}, z\right) + J\left(x, \frac{\partial^2 z}{\partial t \partial z_L}\right) + \frac{\partial}{\partial x_L}J\left(\frac{\partial z}{\partial t}, z\right) + \frac{\partial}{\partial z_L}J\left(x, \frac{\partial z}{\partial t}\right)\right], \tag{A 7}$$

$$\frac{\partial x}{\partial x_L} + \frac{\partial z}{\partial z_L} = -J(x, z). \tag{A 8}$$

The linear solutions are formally identical to the Eulerian solutions, and their derivation is well documented in the literature (e.g. Hansen & Ahmad 1971; Weber & Saetra 1995). When the linear solutions are inserted in the mean momentum equations we obtain to the lowest order

$$\frac{\partial^2 \overline{x}}{\partial t^2} - \nu\frac{\partial^3 \overline{x}}{\partial t \partial z_L^2} = -Q - \nu u_0 k^2 \left\{4\,\mathrm{e}^{2kz_L} + 6\frac{\gamma^2}{k^2}\frac{\mathscr{E}^2}{F}\,\mathrm{e}^{2\gamma z_L} - 4\frac{\gamma^2}{k^2}\left(\frac{\mathscr{E}}{F}\cos\gamma z_L + \frac{\mathscr{E}(1-2\mathscr{E})}{F}\sin\gamma z_L\right)\mathrm{e}^{\gamma z_L}\right\}\mathrm{e}^{-2\alpha x_L}, \tag{A 9}$$

where Q is an unknown pressure gradient force independent of the vertical coordinate, and $\mathscr{E}$ corresponds to the elasticity parameter for the wavenumber k. The particular solution to this equation (with $Q = 0$) yields both the Stokes drift and the boundary layer solution. If we make the partition $\partial\overline{x}/\partial t = U^{(E)} + U^{(p)}$, where the latter part is the particular solution, we find that the quasi-Eulerian part $U^{(E)}$ is governed by

$$\frac{\partial U^{(E)}}{\partial t} - \nu\frac{\partial^2 U^{(E)}}{\partial z_L^2} = -Q. \tag{A 10}$$

This is in essence the same equation as (2.28). For a freely drifting slick, the dynamic surface boundary condition is (e.g. Weber & Saetra 1995)

$$\rho\nu\left[\frac{\partial U^{(E)}}{\partial z_L} + \frac{\partial U^{(p)}}{\partial z_L} + H(\tilde{x}, \tilde{z}, \tilde{p})\right] = -\frac{\partial\overline{\sigma}}{\partial x_L}, \qquad z_L = 0. \tag{A 11}$$

Here H is a nonlinear contribution from the wave solutions (marked with a tilde). This boundary condition expresses that the shear stress and the wave-induced stress at the surface must be balanced by the mean surface tension gradient. Equation (A 11) can be rewritten using the virtual wave stress τ according to the definition

$$\tau = -\rho\nu\left(\frac{\partial U^{(p)}}{\partial z_L}(z_L = 0) + H(\tilde{x}, \tilde{z}, \tilde{p})\right). \tag{A 12}$$

By explicitly calculating the terms on the right-hand side of this equation, which only depends on the wave solutions, we obtain (2.34).

REFERENCES

Alpers, W. & Hühnerfuss, H. 1988 Radar signatures of oil films floating on the sea surface and the Marangoni effect. *J. Geophys. Res.* **93** (C4), 3642–3648.

Andrews, D. G. & McIntyre, M. E. 1978 An exact theory of nonlinear waves on a Lagrangian-mean flow. *J. Fluid Mech.* **84**, 609–646.

ASCE (Task committee on Modeling of Oil Spills). 1996 State-of-the-art review of modeling transport and fate of oil spills. *J. Hydr. Engng* **122** (11), 594–609.

Balk, A. M. 2006 Wave turbulent diffusion due to the doppler shift. *J. Stat. Mech.* 1–13. doi:10.1088/1742-5488/2006/p08018.

Broström, G., Christensen, K. H. & Weber, J. E. 2008 A quasi-eulerian, quasi-lagrangian view of surface-wave-induced flow in the ocean. *J. Phys. Oceanogr.* **38** (5), 1122–1130.

Christensen, K. H. 2005 Transient and steady drift currents in waves damped by surfactants. *Phys. Fluids* **17**, 042102.

Christensen, K. H. & Weber, J. E. 2005*a* Drift of an inextensible sheet caused by surface waves. *Environ. Fluid Mech.* **5**, 495–505.

Christensen, K. H. & Weber, J. E. 2005*b* Wave-induced drift of large floating sheets. *Geophys. Astro. Fluid Dyn.* **99**, 433–443.

Craik, A. D. D. 1982 The drift velocity of water waves. *J. Fluid Mech.* **116**, 187–205.

Dorrestein, R. 1951 General linearized theory of the effect of surface films on water ripples. *Proc. K. Ned. Akad. Wet., Ser.* B*: Phys. Sci.* B **54**, 260–272, 350–356.

Gaster, M. 1962 A note on the relationship between temporally increasing and spatially increasing disturbances in hydrodynamic stability. *J. Fluid Mech.* **14**, 222–224.

Gushchin, L. A. & Ermakov, S. A. 2003 Laboratory study of surfactant redistribution in the flow field induced by surface waves. *Izvestiya Atmos. Oceanic Phys.* **40** (2), 244–249.

Hansen, R. S. & Ahmad, J. 1971 Waves at interfaces. In *Progress in surface and membrane science*, (ed. J. F. Danielli, M. D. Rosenberg & D. A. Cadenhead), vol. 4, pp. 1–56. Academic Press.

Harper, J. F. & Dixon, J. N. 1974 The leading edge of a surface film on contaminated flowing water. In *Fifth Australasian Conference on Hydraulics and Fluid Mechanics*, Christchurch, New Zealand, pp. 499–505.

Herterich, K. & Hasselmann, K. 1982 The horizontal diffusion of tracers by surface-waves. *J. Phys. Oceanogr.* **12** (7), 704–711.

Jenkins, A. D. 1989 The use of a wave prediction model for driving a near-surface current model. *D. Hydrogr. Z.* **42**, 133–149.

Jenkins, A. D. & Ardhuin, F. 2004 Interaction of ocean waves and currents: how different approaches may be reconciled. *ISOPE Proc.* **3**, 105–111.

Lamb, H. 1932 *Hydrodynamics*. Cambridge University Press.

Law, A. W. K. 1999 Wave-induced surface drift of an inextensible thin film. *Ocean Engng* **26**, 1145–1168.

Longuet-Higgins, M. S. 1953 Mass transport in water waves. *Philos. Trans. R. Soc., Ser.* A **245**, 535–581.

Longuet-Higgins, M. S. 1969 A nonlinear mechanism for the generation of sea waves. *Proc. R. Soc.* A **311**, 371–389.

Longuet-Higgins, M. S. 1986 Eulerian and Lagrangian aspects of surface waves. *J. Fluid Mech.* **173**, 683–707.

Lucassen, J. 1968 Longitudinal capillary waves. *Trans. Faraday Soc.* **64**, 2221–2235.

Lucassen-Reynders, E. H. & Lucassen, J. 1969 Properties of capillary waves. *Adv. Colloid Interface Sci.* **2**, 347–395.

Marmorino, G. O., Smith, G. B., Toporkov, J. V., Sletten, M. A., Perkovic, D. & Frasier, S. J. 2008 Evolution of ocean slicks under a rising wind. *J. Geophys. Res.* **113** (C4), C04030. doi:10.1029/2007JC004538.

Mass, J. T. & Milgram, J. H. 1998 Dynamic behavior of natural sea surfactant films. *J. Geophys. Res.* **103**, 15695–15715.

McIntyre, M. E. 1988 A note on the divergence effect and the Lagrangian-mean surface elevation in periodic water waves. *J. Fluid Mech.* **189**, 235–42.

McWilliams, J. C., Sullivan, P. P. & Moeng, C. H. 1997 Langmuir turbulence in the ocean. *J. Fluid Mech.* **334**, 1–30.

Melsom, A. 1992 Wave-induced roll motion beneath an ice cover. *J. Phys. Oceanogr.* **22** (1), 19–28.

Mockros, L. F. & Krone, R. B. 1968 Hydrodynamic effects on an interfacial film. *Science* **161**, 361–363.

Phillips, O. M. 1977 *The Dynamics of the Upper Ocean*. Cambridge University Press.

Pierson, W. J. 1962 Perturbation analysis of the Navier–Stokes equations in Lagrangian form with selected linear solutions. *J. Geophys. Res.* **67** (8), 3151–3160.

Pollard, R. T. 1970 Surface waves with rotation: an exact solution. *J. Geophys. Res.* **75** (30), 5895–5898.

Polton, J. A. & Belcher, S. E. 2007 Langmuir turbulence and deeply penetrating jets in an unstratified mixed layer. *J. Geophys. Res.* **112** (C9), C09020. doi:10.1029/2007JC004205.

Rusanov, V. V. 1961 Calculation of interaction of non-steady shock waves with obstacles. *J. Comput. Math. Phys. USSR* **1**, 267–279.

Saetra, Ø. 1998 Effects of surface film on the linear stability of an air-sea interface. *J. Fluid Mech.* **357**, 59–81.

Vogel, M. J. & Hirsa, A. H. 2002 Concentration measurements downstream of an insoluble monolayer front. *J. Fluid Mech.* **472**, 283–305.

Vucelja, M., Falkovich, G. & Fouxon, I. 2007 Clustering of matter in waves and currents. *Phys. Rev.* E **75** (6), 065301–1.

Weber, J. E. 1983 Attenuated wave-induced drift in a viscous rotating ocean. *J. Fluid Mech.* **137**, 115–129.

Weber, J. E. 2001 Virtual wave stress and mean drift in spatially damped surface waves. *J. Geophys. Res.* **106**, 11653–11657.

Weber, J. E. 2003 Wave-induced mass transport in the oceanic surface layer. *J. Phys. Oceanogr.* **33**, 2527–2533.

Weber, J. E. H., Broström, G. & Saetra, Ø. 2006 Eulerian vs lagrangian approaches to the wave-induced transport in the upper ocean. *J. Phys. Oceanogr.* **36**, 2106–2118.

Weber, J. E. & Saetra, Ø. 1995 Effect of film elasticity on the drift velocity of capillary-gravity waves. *Phys. Fluids* **7**, 307–314.

Welander, P. 1963 On the generation of wind streaks on the sea surface by the action of a surface film. *Tellus* **15**, 67–71.

Wong, P. C. Y. & Law, A. W. K. 2003 Wave-induced drift of an elliptical surface film. *Ocean Engng* **30**, 413–436.